

# Linarite – a quasi-critical $J_1$ - $J_2$ chain

Eron Cemal,<sup>1,2</sup> Mechthild Enderle,<sup>1</sup> Reinhard K. Kremer,<sup>3</sup> Björn Fåk,<sup>1</sup> Eric Ressouche,<sup>4</sup> Mariya V. Gvozdikova,<sup>1</sup> Mike E. Zhitomirsky,<sup>5</sup> and Tim Ziman<sup>1,6</sup>

<sup>1</sup>*Institut Laue-Langevin, CS 20156, 38042 Grenoble Cedex 9, France*

<sup>2</sup>*Royal Holloway, University of London, Egham, Surrey, TW20 0EX, United Kingdom*

<sup>3</sup>*Max-Planck Institute for Solid State Research, Heisenbergstrasse 1, 70569 Stuttgart, Germany*

<sup>4</sup>*Université Grenoble Alpes, CEA, INAC, MEM, F-38000 Grenoble, France*

<sup>5</sup>*Université Grenoble Alpes, CEA, INAC-PHELIQS, F-38000 Grenoble, France*

<sup>6</sup>*LPMMC, UMR-5493, Université Grenoble Alpes and CNRS, 38042 Grenoble, France*

(Dated: January 9, 2018)

The mineral linarite,  $\text{PbCuSO}_4(\text{OH})_2$ , is a spin 1/2 chain with frustrating nearest neighbor ferromagnetic and next-nearest neighbor antiferromagnetic exchange interactions. Our inelastic neutron scattering experiments performed above the saturation field establish that the ratio between these exchanges is such that linarite is extremely close to the quantum critical point between spin-multipolar phases and the ferromagnetic state. We show that the predicted quantum multipolar phases are fragile and actually suppressed by a tiny orthorhombic exchange anisotropy and weak interchain interactions in favor of a dipolar fan phase. Including this anisotropy in classical simulations of a nearly critical model explains the field-dependent phase sequence of the phase diagram of linarite, its strong dependence of the magnetic field direction, and the measured variations of the wave vector as well as the staggered and the uniform magnetizations in an applied field.

Interacting spin-1/2 systems provide a rich source of remarkable discoveries due to the intricate nature of quantum many-body physics. While interacting semiclassical spins  $S \gg 1/2$  tend to arrange themselves into periodic magnetic structures with a finite dipole moment at each site, the quantum character of  $S = 1/2$  spins may lead to disordered spin liquid ground states [1, 2]. Such quantum spin liquids are prone to appear in the vicinity of critical points between vastly different ground states [3]; examples are spin liquids at the boundary between dimerization and long-range magnetic order [4] and the multitude of chiral quantum spin liquids emerging between different types of long-range order on the kagome lattices [5]. Of particular interest are spin models with frustrated ferro- and antiferromagnetic couplings, which have unusual spin-multipolar quantum phases stabilized by an external magnetic field in the proximity of a ferromagnetic ground state [6–16]. The quantum spin-multipolar phases have entangled spin multipoles extending over two or more lattice sites in addition to the incomplete uniform alignment of the spin dipole moments parallel to the field.

In spin-1/2 chains with nearest-neighbor (NN) ferromagnetic (FM) and next-nearest-neighbor (NNN) antiferromagnetic (AFM) interactions, the transverse spin-multipolar quasi-long range order is accompanied by longitudinal spin-dipolar quasi-long-range order with an incommensurate propagation vector  $k_{\text{ic}} = \frac{1}{2p}(1-m)$ , where  $m$  is the uniform moment per site and  $p = 2, 3, \dots$  for quadrupolar, octupolar,  $\dots$  spin tensors, respectively [7–10, 17]. The dipolar correlations of the  $p$ -spin density wave (p-SDW) can be probed in neutron scattering experiments as demonstrated in  $\text{LiCuVO}_4$ , where pair-correlations with incommensurate propagation vec-

tor  $k_{\text{ic}} = \frac{1}{4}(1-m)$  ( $p = 2$ ) and spins parallel to the field have been observed [18]. The existence of spin-multipolar bond order with  $p > 2$ , however, is far less obvious and might depend on the presence of the spin rotational  $U(1)$  symmetry about the field direction [10, 15, 19]. In this context, the mineral linarite plays a particular role: It has been established that the ratio of NN-FM and NNN-AFM exchange [20, 21] is closer to the critical value than in  $\text{LiCuVO}_4$  [22, 23]. In addition, the propagation vector does not follow the simple relation  $k_{\text{ic}} = \frac{1}{2p}(1-m)$  [24], and the reported complex phase diagram [20, 25–27] has remained unexplained.

In this Letter, we combine magnetization and neutron diffraction measurements with zero-temperature simulations of a  $S = 1/2$  model to show that a tiny orthorhombic anisotropy and weak interchain interactions explain the topology of the phase diagram of linarite for three orthogonal field directions as well as the variations of the ordering wave vector in high magnetic fields. Using inelastic neutron scattering (INS) in a strong magnetic field we determine the ratio of the NN and NNN exchange constants and establish unambiguously that linarite is indeed extremely close to the critical point. These results imply that weak anisotropies have a dramatic influence on the field-dependent phase diagram and stabilize ordered dipolar states, raising doubts about the possibility of spin-octupolar or higher multipolar ordering in linarite, and in real materials in general.

Linarite with chemical composition  $\text{PbCuSO}_4(\text{OH})_2$  crystallizes in the space group  $\text{P}2_1/\text{m}$  with  $\beta = 102.65^\circ$  (see [28–32] and Supplemental Material [33]). The crystal structure contains strongly buckled chains of edge-sharing  $\text{CuO}_4$  plaquettes running along the monoclinic  $b$  axis. Like many  $\text{CuO}_2$ -ribbon compounds, it orders at

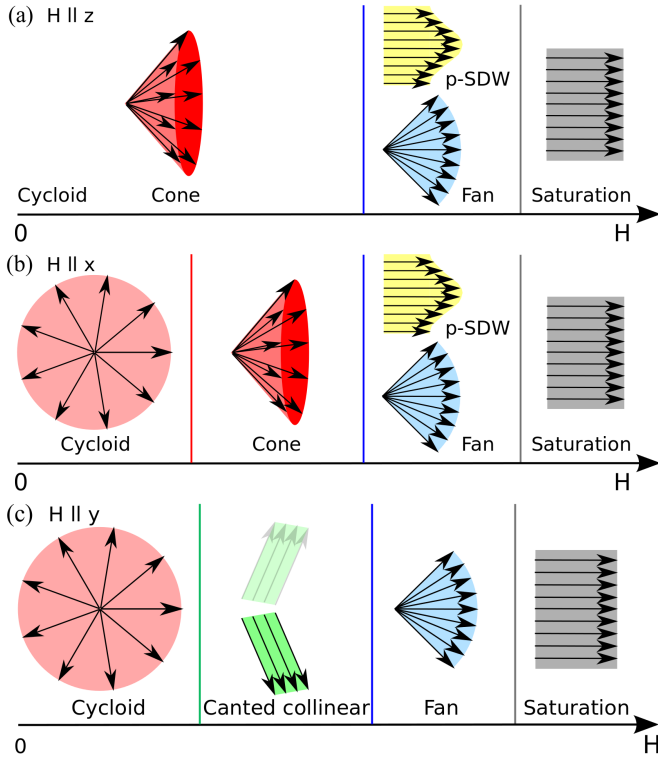


FIG. 1. Schematic phase sequence of quasi-one dimensional spin arrays with NN ferromagnetic and NNN antiferromagnetic intrachain exchange in the vicinity of the quantum critical point. In presence of interchain interactions, p-SDW stands for  $p$ -type quantum spin-density wave states or spin-multipolar bond order. SU(2)-symmetric exchange leads to the phase sequence (a) with a p-SDW phase for all magnetic field directions. U(1)-symmetric exchange of easy-plane type implies sequence (a) for a magnetic field along the symmetry axis (hard axis) and (b) for a field direction in the easy plane, with p-SDW-phases close to saturation ( $p = 2$ ). In linarite, we observe the phase sequence (a) with field along the hardest axis  $H||z$ , (b) with field along the easiest axis  $H||x$ , and (c) for field along the intermediate axis  $H||y||b$ , with dipolar fan phases instead of p-SDW phases close to saturation.

zero magnetic field into a cycloidal magnetic structure with incommensurate propagation vector  $\mathbf{k}$  and simultaneous ferroelectricity. In linarite the cycloid plane is roughly perpendicular to the  $\text{CuO}_4$  plaquettes and contains the  $b$  axis [20], while  $\mathbf{k} = (0, 0.19, \frac{1}{2})$  and  $T_N = 2.8$  K [27, 34]. For convenience we introduce an orthogonal  $xyz$ -spin coordinate system, where  $x$  and  $y$  are in the spin-cycloid plane with  $y||b$  and  $z$  is perpendicular to the cycloid plane. The magnetic field-temperature ( $H$ - $T$ ) phase diagram has been studied with various techniques for magnetic field directions parallel and perpendicular to  $b||y$  [20, 26, 27], but not along  $x$ . The presence of only one zero-field transition implies an easy-plane type anisotropy as the largest deviation from isotropic exchange, leading to schematic phase diagrams as shown in Figs. 1(a) and 1(b) and as observed in  $\text{LiCuVO}_4$  [18, 35].

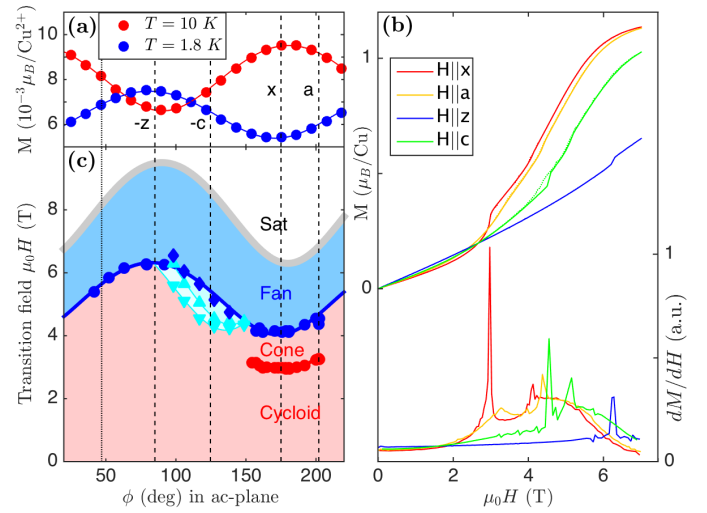


FIG. 2. (a) Magnetization  $M$  as a function of rotation angle in the  $ac$  plane at  $T = 9.995(1)$  K and  $T = 1.830(3)$  K for  $\mu_0 H = 100$  Oe. The longest axis of the  $g$ -tensor (maximum of  $M$  at 10 K) and the spin-plane axis  $x$  are less than  $10^\circ$  apart. (b) Representative  $M(H)$  curves at  $T = 1.8$  K, with their derivatives. Solid curves indicate raising field, dotted lowering field. (c) Phase diagram as a function of rotation angle in the  $ac$  plane and field strength  $\mu_0 H$  at  $T = 1.8$  K. The spin-flop between cycloid and cone phase occurs close to the  $x$  axis. Near the  $c$  axis, a small unknown phase separates the cone and fan phases with a hysteresis at its lower boundary.

However, linarite exhibits an extended commensurate phase for  $H||b$  [20, 24] as in Fig. 1(c), in striking resemblance to the mean-field phase diagram of  $\text{MnWO}_4$  [36]. For field directions perpendicular to  $b$ , the commensurate phase appears to be absent [25–27]. This indicates the substantial role of anisotropy in linarite, in stark contrast to recent attempts to model the high-field behavior [24] and zero-field spin dynamics [21] of linarite based on an entirely isotropic Hamiltonian.

Magnetization as a function of the rotation angle around  $b$  with the magnetic field direction in the  $ac$  plane was measured on an untwinned crystal (see Ref. [32, 33]) at  $T = 10$  K, i.e. above the ordering temperature, and at  $T = 1.8$  K in the cycloid phase, see Fig. 2(a). The angular phase shift between  $T = 4$  K and 10 K in our data is negligible,  $1 \pm 1^\circ$ , as it is in the paramagnetic phase for temperatures between 5 and 25 K [37]. Hence, the  $T = 10$  K data reveal the approximate direction of the principal axes of the  $g$  tensor perpendicular to  $b$ . At  $T = 1.8$  K, in the cycloid phase, the susceptibility is dominated by the spin correlations rather than the local  $g$  tensor, and the magnetization is lowest for a field direction in the cycloid plane. Our data show that the cycloid axis  $x$  is very close to the longest axis of the  $g$  tensor, see Fig. 2(a). The orientation of the spin-plane agrees well with the electric polarization [27] and with unpolarised neutron diffraction [20].

Magnetization measurements as a function of magnetic field for different directions in the  $ac$  plane are shown in Fig. 2(b) and the corresponding transitions in Fig. 2(c). For  $H||z$  (orthogonal to the cycloid plane) below saturation, a single step in  $M(H)$  without hysteresis marks the transition from the cone phase to the fan phase, see Fig. 2(b). This phase sequence agrees well with previous magnetization and dielectric data [26, 27]. In an intermediate angular range including the  $c^*$  and  $c$  directions, a minor unknown phase is intercalated between the cone and fan phases [cyan region in Fig. 2(c)], its boundary with the cone phase displaying a large hysteresis, see  $H||c$  in Figs. 2(b) and 2(c). As the field direction approaches the cycloid plane, this minor phase disappears. With  $H||x$ , in the cycloid plane, an S-shaped hysteresis-free magnetization between cycloid and cone phase, the cone-fan transition field is at its minimum (4.1 T), and the saturation is already reached at about 6.3 T. The spin-flop transition also exists for field directions up to about  $\pm 30^\circ$  out of the cycloid plane, see Fig. 2(c), including the crystallographic  $a$  direction. At the angular end points, the spin-flop field reaches 3.3 T.

Neutron diffraction [33] with  $H||a$  at a temperature of 60 mK shows that the propagation vector remains incommensurate  $(0, k_{ic}, \frac{1}{2})$  from zero field up to the saturation field,  $H_{\text{sat}}$ , see Fig. 3(a). At the spin-flop transition  $k_{ic}(H)$  jumps slightly upward, while the magnetic Bragg peak intensity decreases by a factor two, precisely as observed near the spin-flop transitions of  $\text{LiCuVO}_4$  [35]. This is because neutron diffraction at this wave vector senses both cycloid components but only one of the cone components. The propagation vector  $k_{ic}(H)$  decreases as the cone-fan phase transition at  $H \approx 5.5$  T is approached from below but increases above, in stark contrast to the decreasing  $k_{ic}(H)$  expected for a spin-multipolar quantum phase. The intensity displays no anomaly, which means that the visible component of the staggered moment,  $m_b$ , varies smoothly across the transition. The staggered moment vanishes at about  $H = 6.3$  T, while the uniform moment (measured via the intensity of the (200) reflection, not shown) saturates, in agreement with the saturating magnetization, Fig. 2(b). Complementary magnetization and neutron diffraction measurements at  $T \sim 1.5$  K confirm that the spin-flop transition field is nearly temperature-independent, while the cone-fan transition shifts to lower fields and at  $T = 1.8$  K corresponds to the blue line in Fig. 2(c).

For  $H||b$ , our neutron diffraction data at  $T = 60$  mK confirm the major phase sequence observed in magnetization and neutron diffraction at higher temperatures [20, 24]. This is illustrated in Fig. 3(b):  $k_{ic}(H)$  jumps from incommensurate to commensurate values and back to incommensurate. In the fan phase just below saturation we observe – precisely as for  $H||a$  – a continuous increase of  $k_{ic}(H)$  with  $H$  at constant temperature of

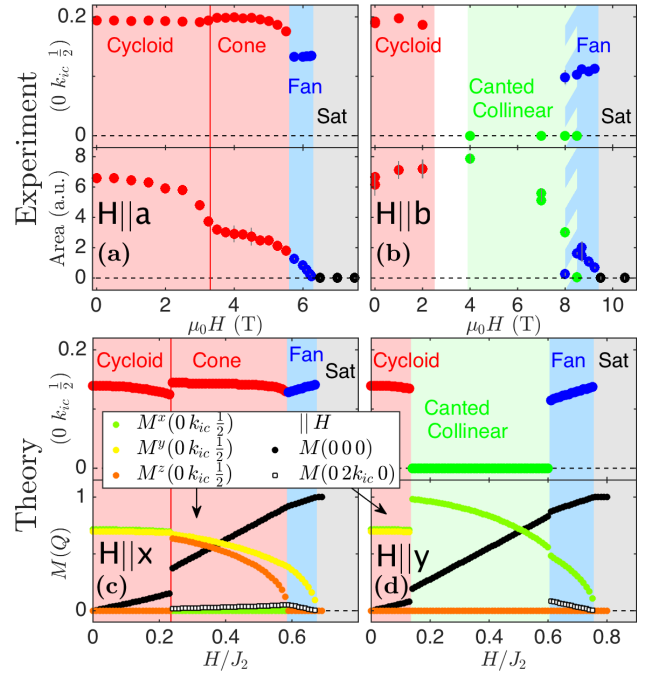


FIG. 3. (a–b) Measured ordering wave vector  $(0, k_{ic}, \frac{1}{2})$  and integrated Bragg peak intensity at  $T = 60$  mK as a function of magnetic field along (a)  $H||a$  and (b)  $H||b$ . The integrated Bragg peak intensity at  $\mathbf{Q}$  (near  $z$ ) is proportional to  $|\mathbf{M}(\mathbf{Q}) - \mathbf{M}(\mathbf{Q})\hat{\mathbf{Q}}|^2$ . (c–d) Calculated ordering wave vector  $(0, k_{ic}, \frac{1}{2})$ , uniform  $\mathbf{M}(0, 0, 0)$  and staggered magnetization amplitudes  $\mathbf{M}(\mathbf{Q})$  at  $T = 0$  as a function of the reduced magnetic field  $H/J_2$  along (c)  $H||x$  (near the  $a$  axis) and (d)  $H||y$  ( $||b$ ).

60 mK, in sharp contrast to the decrease  $k_{ic} \propto (1 - m)/p$  predicted for spin-multipolar quantum phases, and observed in  $\text{LiCuVO}_4$  [18].

The observation of entirely different phase sequences in three orthogonal field directions  $x, y, z$  demonstrates that a bi-axial anisotropy is essential to understand the magnetism of linarite. We therefore introduce a minimal spin-1/2 Hamiltonian

$$\mathcal{H} = J_1 \sum_{\langle ij \rangle}^{NN} \left[ (1 + \delta) S_i^x S_j^x + S_i^y S_j^y + (1 - \epsilon) S_i^z S_j^z \right] + J_2 \sum_{\langle ij \rangle}^{NNN} \mathbf{S}_i \mathbf{S}_j + J_c \sum_{\langle ij \rangle}^{\text{inter}} \mathbf{S}_i \mathbf{S}_j - \mu_B \sum_{i, \alpha} g_{\alpha\alpha} H^\alpha S_i^\alpha \quad (1)$$

with orthorhombic anisotropy included on the strongest ferromagnetic NN bond  $J_1 < 0$ . A significant second-neighbor coupling  $J_2 > 0$  beyond the critical ratio  $J_2/J_1 = -1/4$  produces the incommensurate spiral structure along the chain  $b$  direction, whereas  $J_c > 0$  between direct neighbors in the  $c$  direction, see Fig. 4, assures an antiferromagnetic spin arrangement in this direction with an overall propagation wave vector  $(0, k_{ic}, \frac{1}{2})$ , as observed in linarite. We further neglect a mismatch between the principal axes of the  $g$  tensor and the principal axes of the

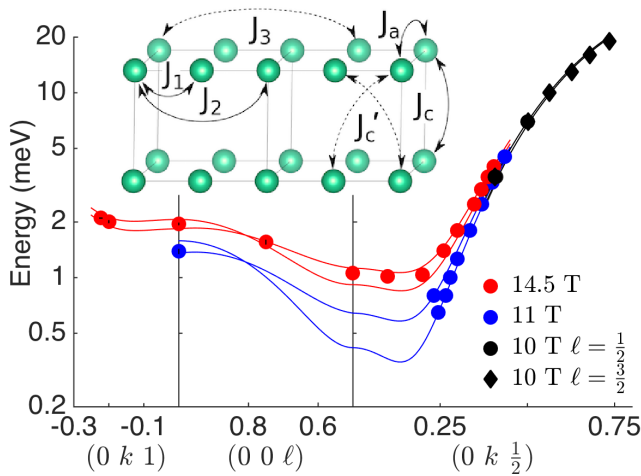


FIG. 4. Dispersion of linearite for  $H||a$  with  $H > H_{sat}$  (symbols) and spin-wave fit (lines) to the two twins. The inset displays the interaction scheme with  $\text{Cu}^{2+}$  in two unit cells in the  $b$ -direction. Relevant interactions are shown as solid lines, additionally considered interactions as dashed lines.

main exchange, since our magnetization measurements above and below  $T_N$  show that the mismatch is small, see Fig. 2(a). The antisymmetric Dzyaloshinski-Moriya interaction (DM) can play only a subsidiary role, since in Eq. (1), DM is allowed only on  $J_1$  from space group symmetry, and thus cannot account for bi-axial anisotropy [33].

We investigate the competition between incommensurability and anisotropy described by (1) using real-space mean-field simulations [36] at zero temperature, which for  $S = 1/2$  is equivalent to the classical minimization. This approach is justified by the large size of the ordered magnetic moments in linearite in zero magnetic field,  $1.05\mu_B$  [20], which indicates the weakness of quantum effects in presence of anisotropy and inter-chain interaction. Further details of the approach are explained in [33]. The general qualitative behavior of the equilibrium magnetic structure described by (1) is as follows. In zero field, an easy-plane anisotropy  $\epsilon > 0$  stabilizes the cycloid in the  $xy$  plane with a propagation vector  $\cos(\pi k_{ic}) = -J_1/(4J_2)$ . The in-plane magnetic field  $\mathbf{H} || x, y$  induces a spin-flop transition into a distorted conical state, cf. Fig. 1(b). For small  $k_{ic}$ , a small in-plane anisotropy  $\delta > 0$  is sufficient to suppress the spin-flop for  $\mathbf{H} || y$  replacing it with a transition into a canted commensurate state with the staggered moments oriented along the easy axis  $\mathbf{M}(0, k_{ic}, \frac{1}{2}) || x$ , cf. Fig. 1(c). For  $H||z$ , the cone phase is stable from zero field to near saturation, cf. Fig. 1(a). For all three field orientations, the saturated phase is preceded by an incommensurate fan phase. The absence of rotational symmetry in the spin Hamiltonian (1) leads to variations of the propagation vector in a magnetic field, which are most pro-

nounced in the fan state, corroborating previous theoretical work [38].

Detailed comparison with the experimental results shown in Fig. 3(a,b) have been made for a set of parameters relevant for linearite:  $|J_1^{yy}/J_2| = 3.62$ ,  $|J_c/J_2| = 0.17$ ,  $\epsilon = 0.01$ ,  $\delta = 0.005$ , and  $g = 2$ , see Fig. 3(c,d). The obtained phase sequences match the major observed phases for all three field directions sketched in Fig. 1. The calculation reproduces correctly numerous qualitative features, such as the variation of the wave vector as a function of the magnetic field [upper parts in Fig. 3(c,d) versus (a,b)] or the type of anomaly of the staggered and uniform magnetizations at the phase transitions shown in the lower part of Fig. 3(c,d). The uniform magnetization  $\mathbf{M}(0, 0, 0)$  in Fig. 3(c,d) compares directly to Fig. 2(b) and Ref.[26]; the theoretical  $[M^x(\mathbf{Q})]^2 + [M^y(\mathbf{Q})]^2$  of Fig. 3(c,d) matches the experimental Bragg peak intensity at  $\mathbf{Q} = (0, k_{ic}, \frac{1}{2})$  near  $z$  in Fig. 3(a,b) (see also [33]).

The excellent qualitative agreement between theory and experiment, and notably the increasing  $k_{ic}(H)$  with field, see Fig. 3, identifies the high-field phases of linearite as fan phases, in contrast to spin-multipolar quantum phases that should feature a decreasing  $k_{ic} \propto (\frac{1}{2} - m)/p$ . Since  $k_{ic}(H)$  increases with field close to saturation for two perpendicular field directions in the cycloid plane at a constant temperature of  $T = 60$  mK, we can rule out a succession of spin-multipolar phases [24]. The latter was suggested on the basis of measurements of wave vectors  $k_{ic}(H)$  along lines of varying and rather elevated temperatures (i.e., measurements of  $k_{ic}(H, T)$  rather than  $k_{ic}(H, T \rightarrow 0)$ , see figure 2b in [24] and figures 5.49 and 5.16 in [39]).

In order to establish how close linearite is to the quantum critical point, we have determined the exchange interactions from INS measurements at low temperatures of the spin-wave spectrum above  $H_{sat}$ , where the magnetic moments are aligned parallel to the magnetic field, and hence classical spin-wave theory is applicable. The twinning [32] observed on all large natural crystals of linearite was taken into account explicitly, see [33].

A global fit [40–42] of all data taken at different field strengths (10 T, 11 T, 14.5 T) gives  $J_1 = -14.5(2)$  meV,  $J_2 = 3.93(6)$  meV, direct interchain exchange  $J_c = 0.7(1)$  meV, vanishing  $J_a = -0.1(2)$  meV and diagonal interchain exchange  $J'_c = -0.06(3)$  meV,  $g_a = 2.5(3)$ ,  $g_{twin} = 2.3(3)$ ,  $\epsilon = 0.03(1)$ , and  $\delta < 0.005$ . Our data rule out sizable diagonal interchain exchange ( $J'_c \sim -0.1J_1$ ) that had been supposed in previous interpretations of  $k_{ic}(H, T)$  [24]. The low-energy zero-field dispersion of [21], affected by quantum renormalization [43, 44], is compatible with a wide range of parameters and cannot distinguish between diagonal ( $J'_c$ ) and direct ( $J_c$ ) interchain exchange. Including third-nearest neighbor intra-chain exchange  $J_3$  improves our fit slightly [33]. With or without  $J_3$  linearite is very close to the ferromagnetic

phase boundary in the parameter space [45–47], about an order of magnitude closer than e.g.  $\text{LiCuVO}_4$ .

In conclusion, we find linarite very close to the critical line where ferromagnetism sets in. Our findings demonstrate that at such close proximity to the critical point, tiny anisotropies and interchain interactions are highly relevant and sufficient to suppress higher-order spin-multipolar quantum phases in favor of the observed dipolar fan phase. Indeed, replacement of the  $U(1)$  symmetry by two-fold  $C_2$  rotations mixes all odd magnon sectors preventing the distinction between the ordering of third-rank octupolar spin tensors and usual dipolar ordering. A lower symmetry would even mix odd and even magnon sectors. This implies that in real materials, the stability of quantum spin-multipolar phases in competition with dipolar long-range order is more limited than suspected so far. Our work shows that in the vicinity of the quantum critical point, the dipolar fan phase occurs in the frustrated quantum chain and is stabilized by a tiny orthorhombic anisotropy. We also note that orthorhombic anisotropy can induce ordinary ( $p = 1$ ) spin-density waves and/or fan phases both as a function of temperature and as a function of magnetic field even further away from the critical point [36], where its role has been overlooked so far [48–50].

- 
- [1] Y. Zhou, K. Kanoda, and T.-K. Ng, *Rev. Mod. Phys.* **89**, 025003 (2017).
- [2] L. Savary and L. Balents, *Rep. Prog. Phys.* **80**, 016502 (2017).
- [3] O. A. Starykh, *Rep. Prog. Phys.* **78**, 052502 (2015).
- [4] A. W. Sandvik, *Phys. Rev. Lett.* **98**, 227202 (2007).
- [5] S. Bieri, L. Messio, B. Bernu, and C. Lhuillier, *Phys. Rev. B* **92**, 060407(R) (2015).
- [6] N. Shannon, T. Momoi, and P. Sindzingre, *Phys. Rev. Lett.* **96**, 027213 (2006).
- [7] T. Vekua, A. Honecker, H.-J. Mikeska, and F. Heidrich-Meisner, *Phys. Rev. B* **76**, 174420 (2007).
- [8] L. Kecke, T. Momoi, and A. Furusaki, *Phys. Rev. B* **76**, 060407(R) (2007).
- [9] T. Hikihara, L. Kecke, T. Momoi, and A. Furusaki, *Phys. Rev. B* **78**, 144404 (2008).
- [10] J. Sudan, A. Lüscher, and A. M. Läuchli, *Phys. Rev. B* **80**, 140402(R) (2009).
- [11] F. Heidrich-Meisner, I. P. McCulloch, and A. K. Kolezhuk, *Phys. Rev. B* **80**, 144417 (2009); *Phys. Rev. B* **81**, 179902(E) (2010).
- [12] R. Shindou and T. Momoi, *Phys. Rev. B* **80**, 064410 (2009).
- [13] M. E. Zhitomirsky and H. Tsunetsugu, *Europhys. Lett.* **92**, 37001 (2010).
- [14] H. T. Ueda and K. Totsuka, *Phys. Rev. B* **80**, 014417 (2009).
- [15] L. Balents and O. A. Starykh, *Phys. Rev. Lett.* **116**, 177201 (2016).
- [16] O. Janson, S. Furukawa, T. Momoi, P. Sindzingre, J. Richter, and K. Held, *Phys. Rev. Lett.* **117**, 037206 (2016).
- [17] M. Sato, T. Momoi, and A. Furusaki, *Phys. Rev. B* **79**, 060406(R) (2009).
- [18] M. Mourigal, M. Enderle, B. Fåk, R. K. Kremer, J. M. Law, A. Schneidewind, A. Hiess, and A. Prokofiev, *Phys. Rev. Lett.* **109**, 027203 (2012).
- [19] S. Nishimoto, S. L. Drechsler, R. Kuzian, J. Richter, and J. van den Brink, *Phys. Rev. B* **92**, 214415 (2015); arXiv:1303.1933v1[cond-mat.str-el]
- [20] B. Willenberg, M. Schäpers, K. C. Rule, S. Süllow, M. Reehuis, H. Ryll, B. Klemke, K. Kiefer, W. Schottenhamel, B. Büchner, B. Ouladdiaf, M. Uhlarz, R. Beyer, J. Wosnitza, and A. U. B. Wolter, *Phys. Rev. Lett.* **108**, 117202 (2012).
- [21] K. C. Rule, B. Willenberg, M. Schäpers, A. U. B. Wolter, B. Büchner, S. L. Drechsler, G. Ehlers, D. A. Tennant, R. A. Mole, J. S. Gardner, S. Süllow, and S. Nishimoto, *Phys. Rev. B* **95**, 024430 (2017).
- [22] M. Enderle, C. Mukherjee, B. Fåk, R. K. Kremer, J.-M. Broto, H. Rosner, S.-L. Drechsler, J. Richter, J. Malek, A. Prokofiev, W. Assmus, S. Pujol, J.-L. Raggazzoni, H. Rakoto, M. Rheinstädter, and H. M. Rønnow, *Europhys. Lett.* **70**, 237 (2005).
- [23] M. Enderle, B. Fåk, H.-J. Mikeska, R. K. Kremer, A. Prokofiev, and W. Assmus, *Phys. Rev. Lett.* **104**, 237207 (2010).
- [24] B. Willenberg, M. Schäpers, A. U. B. Wolter, S. L. Drechsler, M. Reehuis, J. U. Hoffmann, B. Büchner, A. J. Studer, K. C. Rule, B. Ouladdiaf, S. Süllow, and S. Nishimoto, *Phys. Rev. Lett.* **116**, 047202 (2016).
- [25] A. U. B. Wolter, F. Lipps, M. Schäpers, S. L. Drechsler, S. Nishimoto, R. Vogel, V. Kataev, B. Büchner, H. Rosner, M. Schmitt, M. Uhlarz, Y. Skourski, J. Wosnitza, S. Süllow, and K.C. Rule, *Phys. Rev. B* **85**, 014407 (2012).
- [26] M. Schäpers, A. U. B. Wolter, S. L. Drechsler, S. Nishimoto, K. H. Müller, M. Abdel-Hafez, W. Schottenhamel, B. Büchner, J. Richter, B. Ouladdiaf, M. Uhlarz, R. Beyer, Y. Skourski, J. Wosnitza, K. C. Rule, H. Ryll, B. Klemke, K. Kiefer, M. Reehuis, B. Willenberg, and S. Süllow, *Phys. Rev. B* **88**, 184410 (2013).
- [27] K.Y. Povarov, Y. Feng, and A. Zheludev, *Phys. Rev. B* **94**, 214409 (2016).
- [28] H. G. Bachmann and J. Zemann, *Acta Cryst.* **14**, 747 (1961).
- [29] T. Araki, *Mineralogical Journal* **3**, 282 (1962).
- [30] H. Effenberger, *Mineralogy and Petrology* **36**, 3 (1987).
- [31] P. F. Schofield, C. C. Wilson, K. S. Knight, and C. A. Kirk, *Canadian Mineralogist* **47**, 649 (2009).
- [32] Twinning on  $\{100\}$  is common according to <http://www.mindat.org>.
- [33] See Supplemental Material.
- [34] Y. Yasui, Y. Yanagisawa, M. Sato, and I. Terasaki, *J. Phys. Conf. Ser.* **320**, 012087 (2011).
- [35] M. Mourigal, M. Enderle, R. K. Kremer, J. M. Law, and B. Fåk, *Phys. Rev. B* **83**, 100409(R) (2011).
- [36] M. V. Gvozdikova, T. Ziman, and M. E. Zhitomirsky, *Phys. Rev. B* **94**, 020406(R) (2016).
- [37] R. Szymczak, H. Szymczak, G. Kamieniarz, G. Szukowski, K. Jasiewicz-Pacer, W. Florek, V. Maltsev, and G. J. Babonas, *Acta Physica Polonica A* **115**, 925 (2009).
- [38] T. Nagamiya, Helical Spin Ordering – 1 Theory of Helical Spin Configurations, in: *Solid State Physics* vol. **20**, 305

- (1967), eds. F. Seitz, D. Turnbull, and H. Ehrenreich, Academic Press, New York and London.
- [39] B. Willenberg, Ground State Properties and Field Induced Phases in Quasi One-Dimensional Quantum Magnets, Dissertation, TU Braunschweig (2013); <http://www.digibib.tu-bs.de/?docid=00055517>.
- [40] S. Toth and B. Lake, *J. Phys.: Condens. Matter* **27**, 166002 (2015).
- [41] F. James and M. Roos, *Computer Physics Commun.* **10**, 343 (1975).
- [42] G. Allodi, Fminuit software package, <http://www.fis.unipr.it/guiseppe.allodi/Fminuit/>.
- [43] R. Coldea, D. A. Tennant, K. Habicht, P. Smeibidl, C. Wolters, and Z. Tylczynski, *Phys. Rev. Lett.* **88**, 137203 (2002).
- [44] J. Ren and J. Sirker, *Phys. Rev. B* **85**, 140410(R) (2012).
- [45] A. Pimpinelli, E. Rastelli, and A. Tassi, *J. Phys.: Condens. Matter* **1**, 7941 (1989).
- [46] R. Zinke, J. Richter, and S. L. Drechsler, *J. Phys.: Condens. Matter* **22**, 446002 (2010).
- [47] T. Nagamiya, K. Nagata, and Y. Kitano, *Progr. Theor. Phys.* **27**, 1253 (1962).
- [48] M. Pregelj, A. Zorko, O. Zaharko, H. Nojiri, H. Berger, L. C. Chapon, and D. Arcon, *Nat. Commun.* **6**, 7255 (2015).
- [49] M. Pregelj, O. Zaharko, M. Herak, M. Gomilsek, A. Zorko, L. C. Chapon, F. Bourdarot, H. Berger, and D. Arcon, *Phys. Rev. B* **94**, 081114 (2016).
- [50] F. Weickert, N. Harrison, B. L. Scott, M. Jaime, A. Leitmäe, I. Heinmaa, R. Stern, O. Janson, H. Berger, H. Rosner, and A. A. Tsirlin, *Phys. Rev. B* **94**, 064403 (2016).